Supporting Information

BODIPY-diketopyrrolopyrrole-porphyrin Conjugate Small Molecules for Use in Bulk Heterojunction Solar Cells

L. Bucher, N. Desbois, E. N. Koukaras, C. H. Devillers, S. Biswas, G. D. Sharma, and C. P. Gros

Table of contents

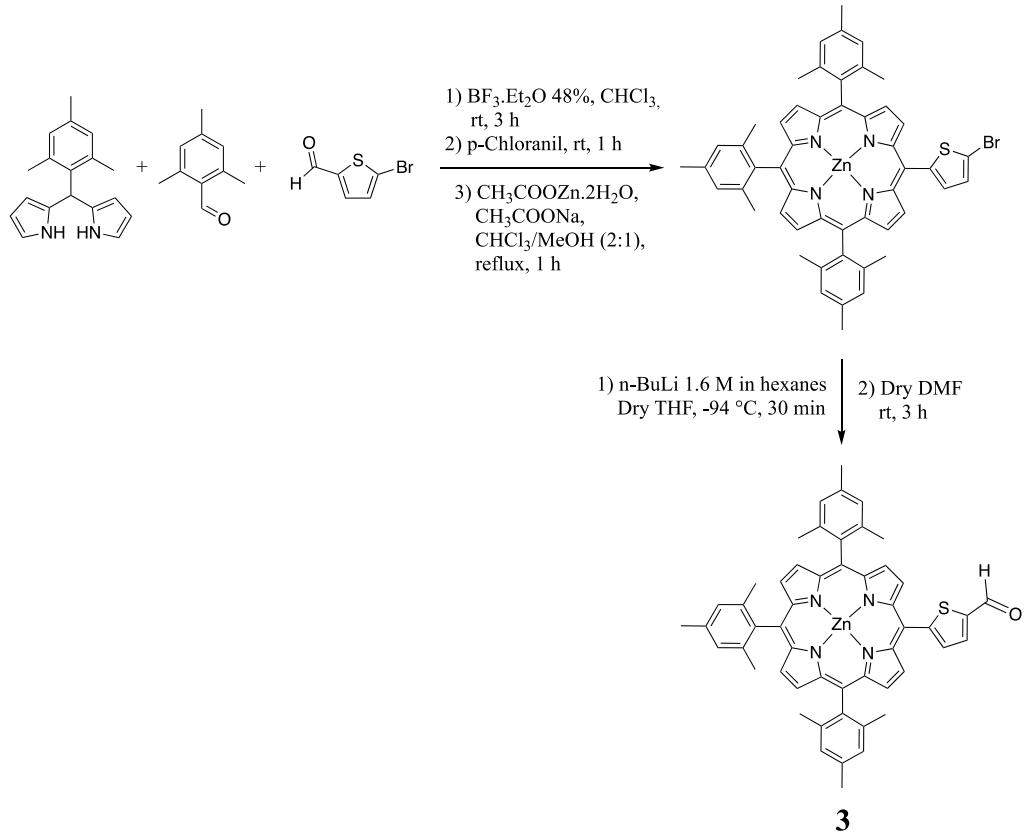

Fig. S1. Synthesis of porphyrin **3**

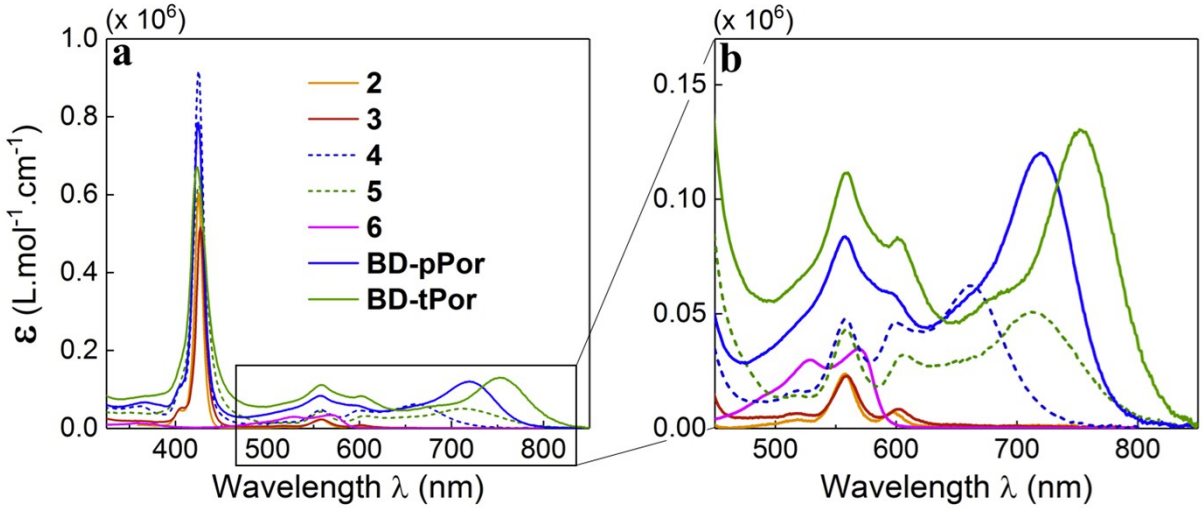

Fig. S2. a) Absorption spectra of all compounds in THF at 298 K, b) zoom on the 560 - 850 nm region

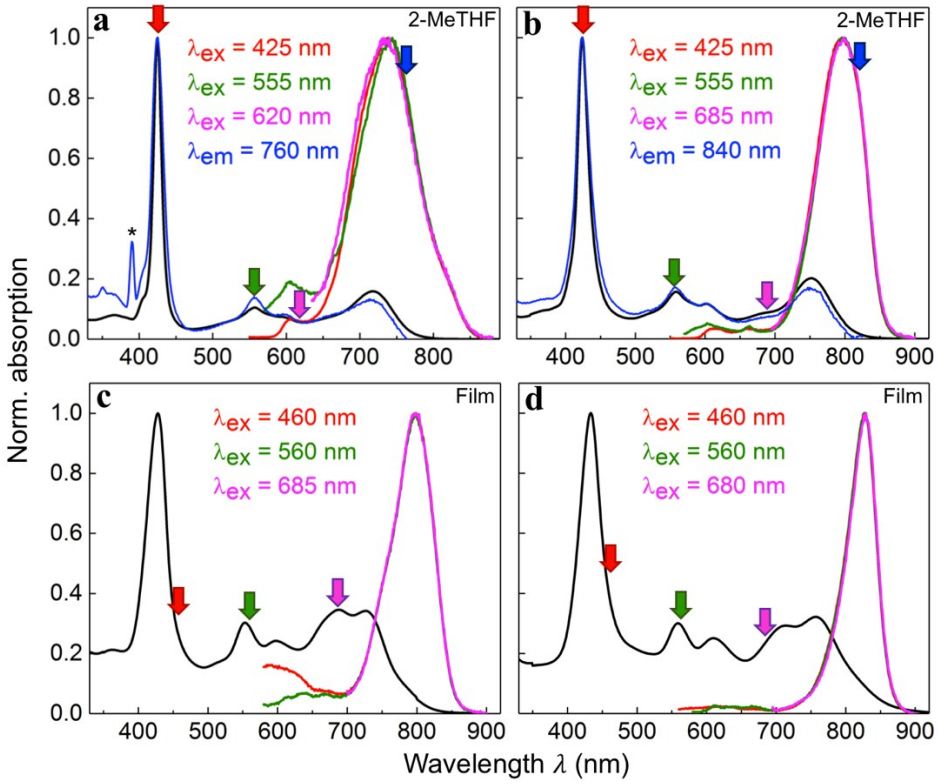

Fig. S3. Absorption (black line), emission (red, green and purple lines) and excitation (blue line) spectra of **BD-pPor (a)** in 2-MeTHF and **(c)** in thin film, and **BD-tPor (b)** in 2-MeTHF and **(d)** in thin film, *artefact from excitation beam ($2\lambda_{ex}$ harmonic)

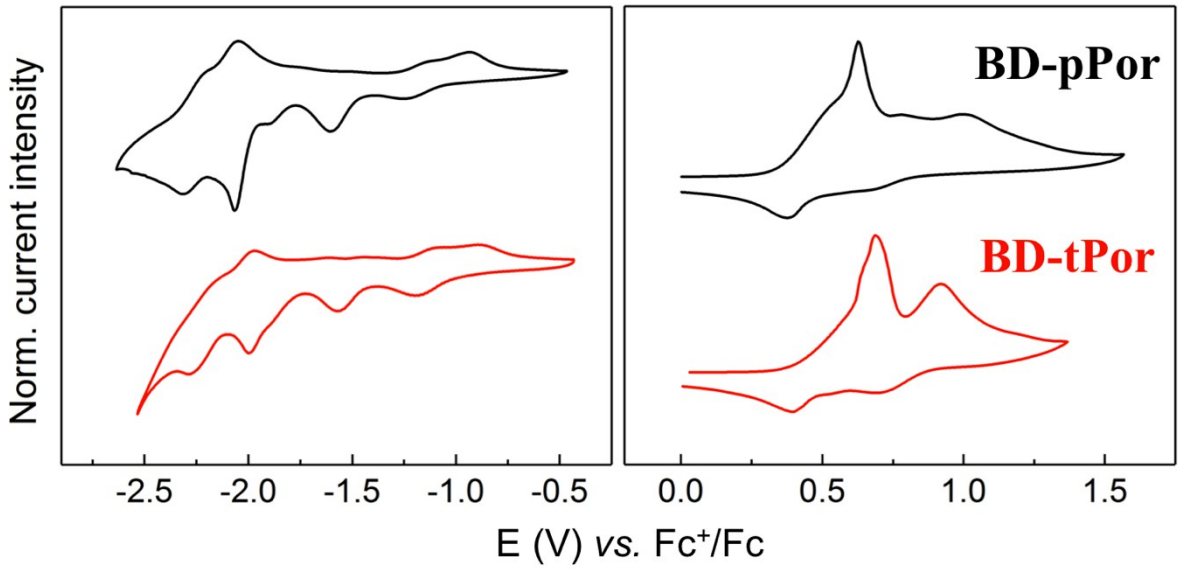

Fig. S4. Cyclic voltammograms of **BD-pPor** (black curve) and **BD-tPor** (red curve) as thin films in 0.1 M $TBAPF_6$ MeCN solution (scan rate = 1 $V.s^{-1}$)

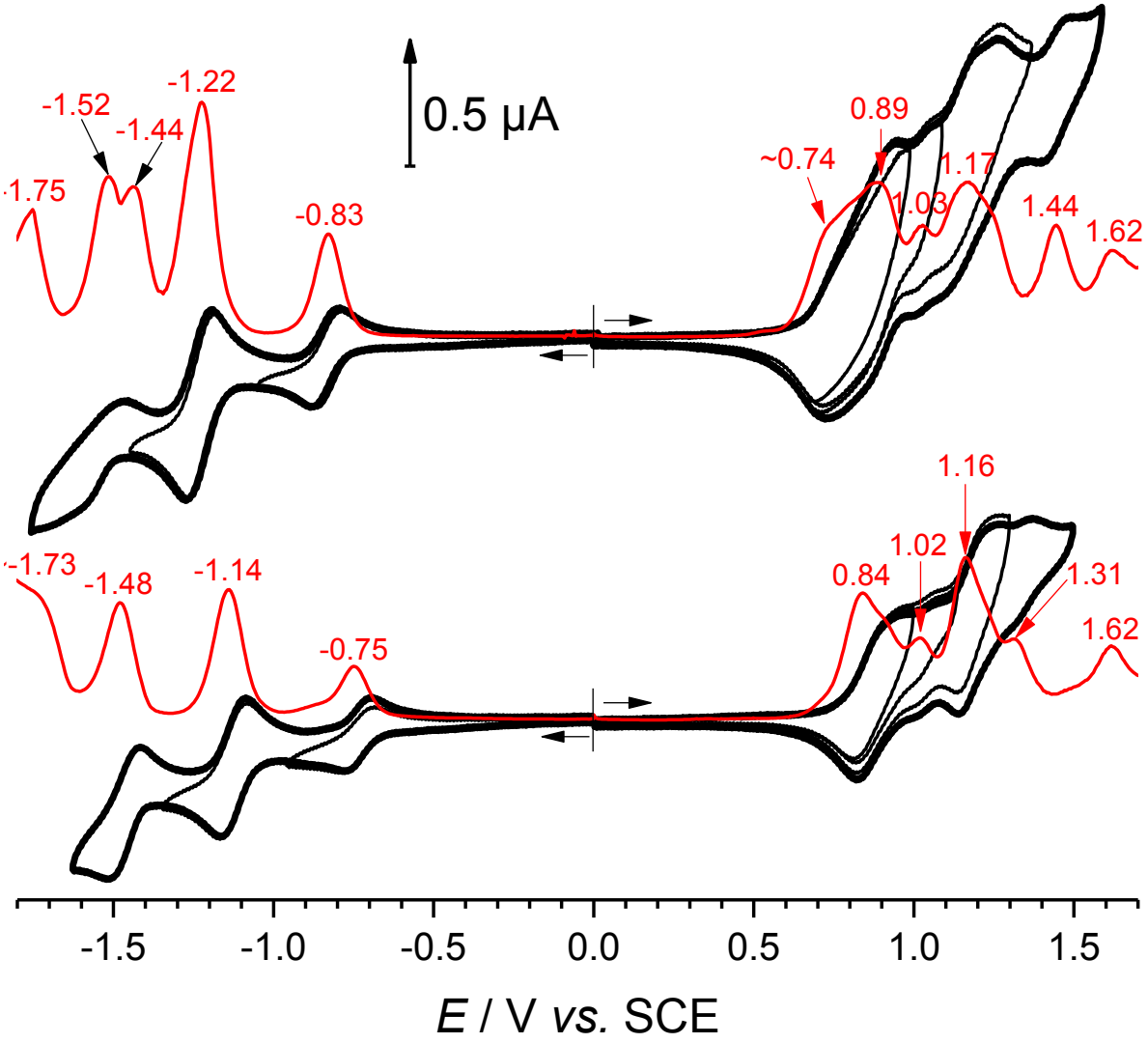

Fig. S5. Cyclic voltammograms (in black) and DPV curves (in red, intensities of all DPV curves have been multiplied by a factor of 2) for **BD-tPor** (top) and **BD-pPor** (bottom) in CH_2Cl_2 0.1 M $TBAPF_6$ ([**BD-tPor**]=4×10^{-4} M and [**BD-pPor**]= 2×10^{-4} M, WE: Pt Ø=1 mm, CE: Pt, RE: SCE, *v* = 100 mV/s (CV) and 10 mV/s (DPV) respectively; subtract 0.46 V to get the potential values *vs.* Fc/Fc^+).

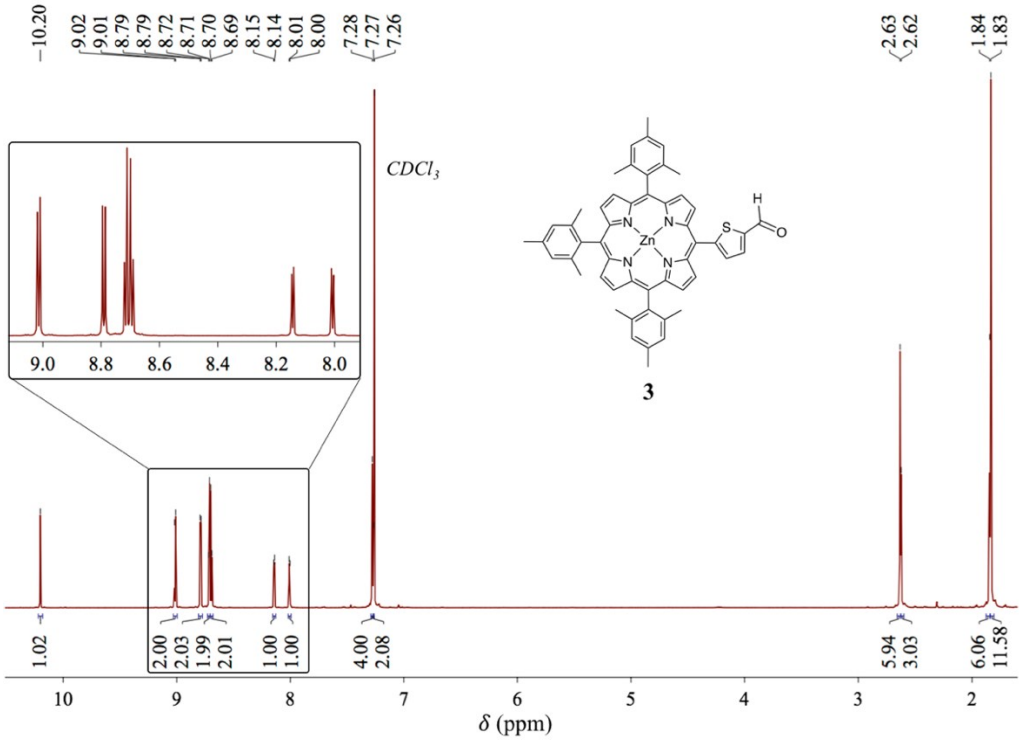

Fig. S6. ^{1}H NMR spectrum ($CDCl_3$, 500 MHz) of porphyrin **3**

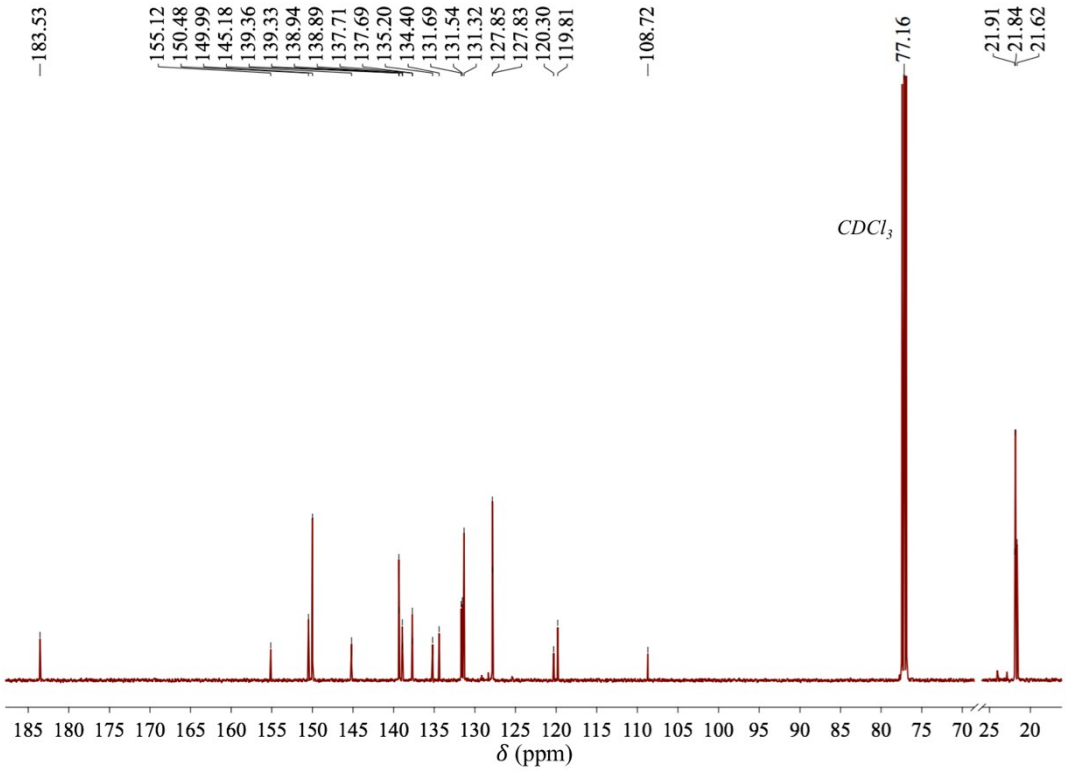

Fig. S7. ^{13}C NMR spectrum ($CDCl_3$, 125 MHz) of porphyrin **3**

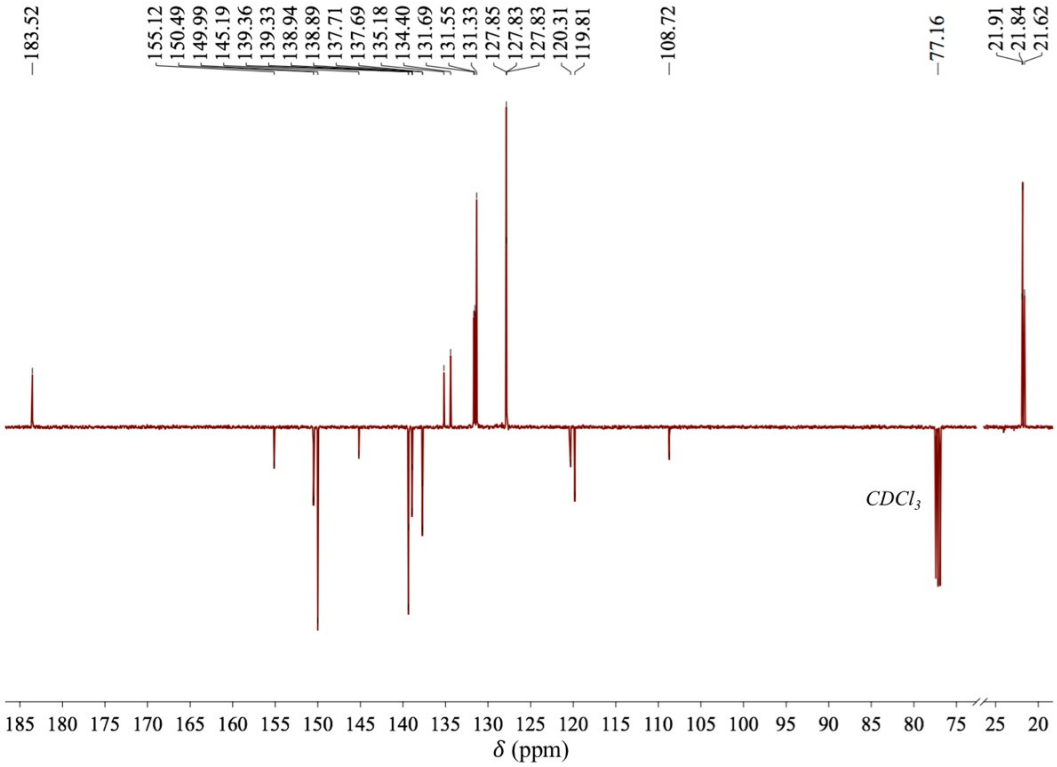

Fig. S8. JMOD ^{13}C NMR spectrum ($CDCl_3$, 125 MHz) of porphyrin **3**

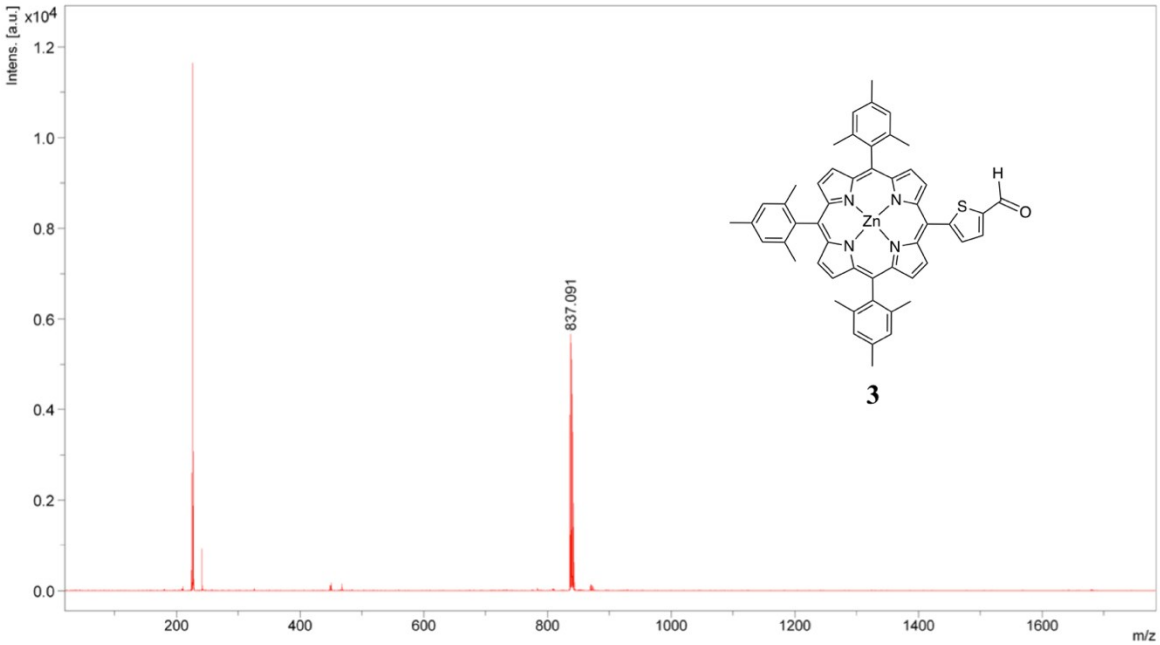

Fig. S9. LRMS MALDI/TOF spectrum of **3** (full)

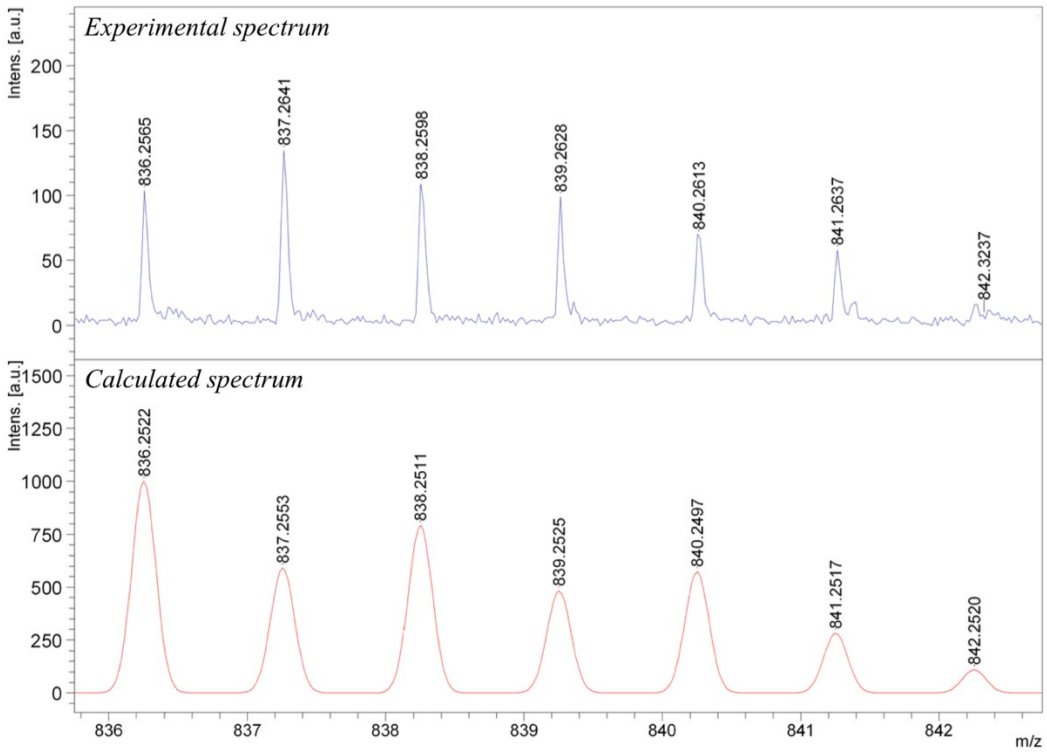

Fig. S10. HRMS MALDI/TOF spectrum of **3** (zoom)

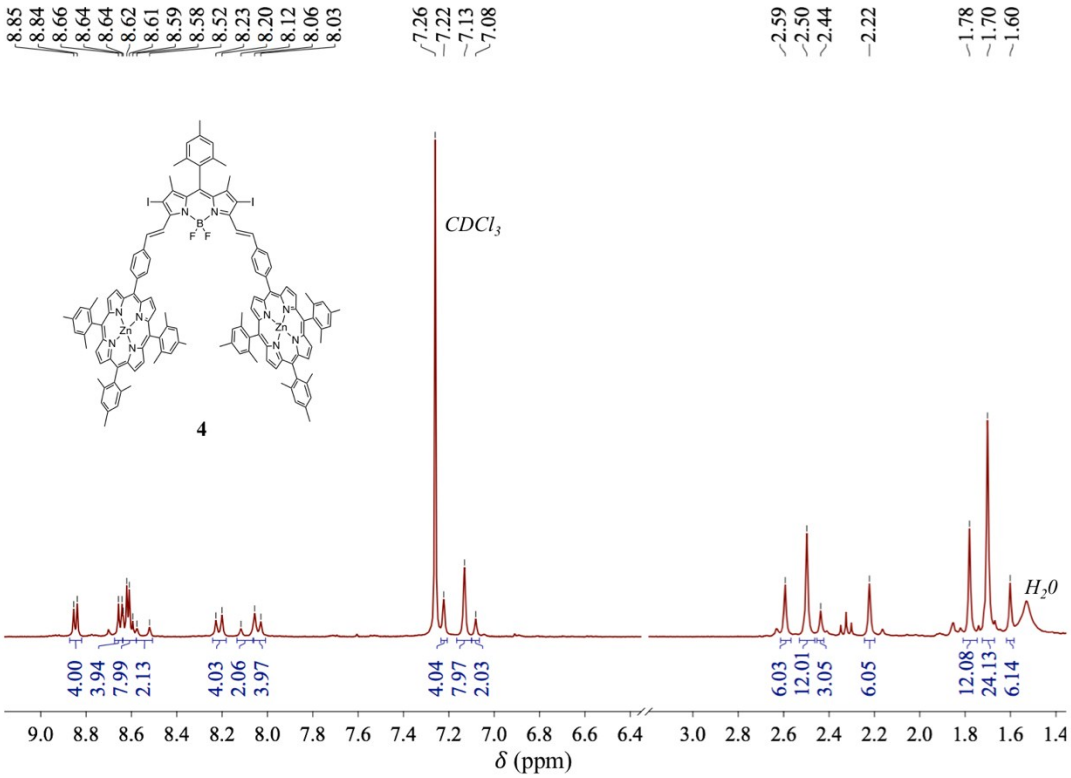

Fig. S11. ^{1}H NMR spectrum ($CDCl_3$, 300 MHz) of **4**

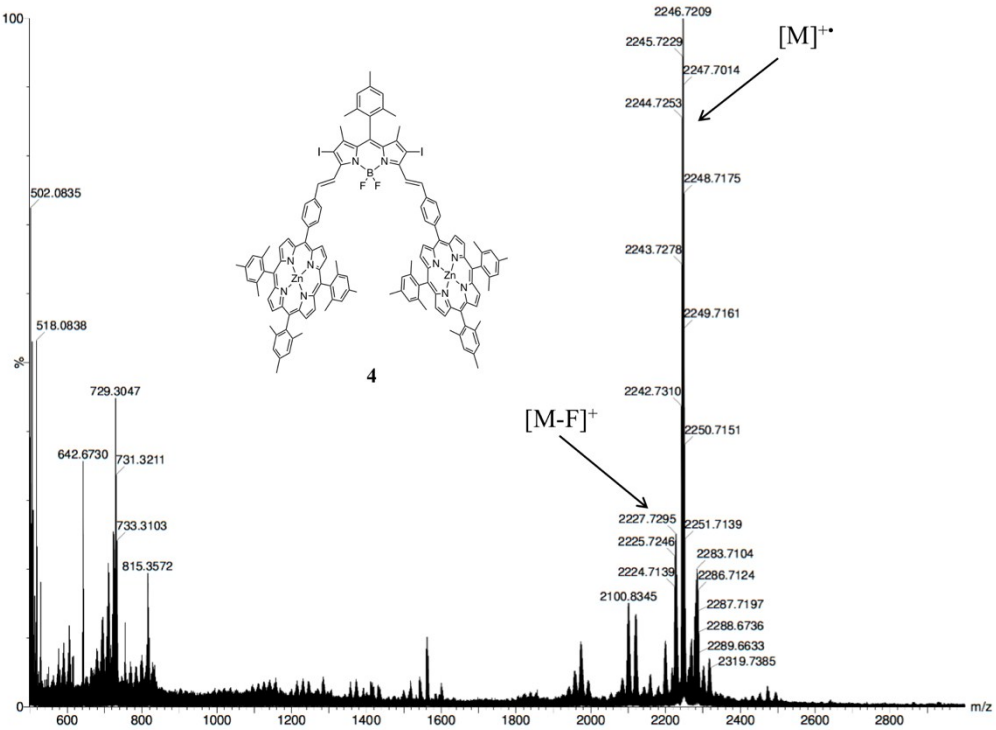

Fig. S12. LRMS MALDI/TOF spectrum of **4** (full)

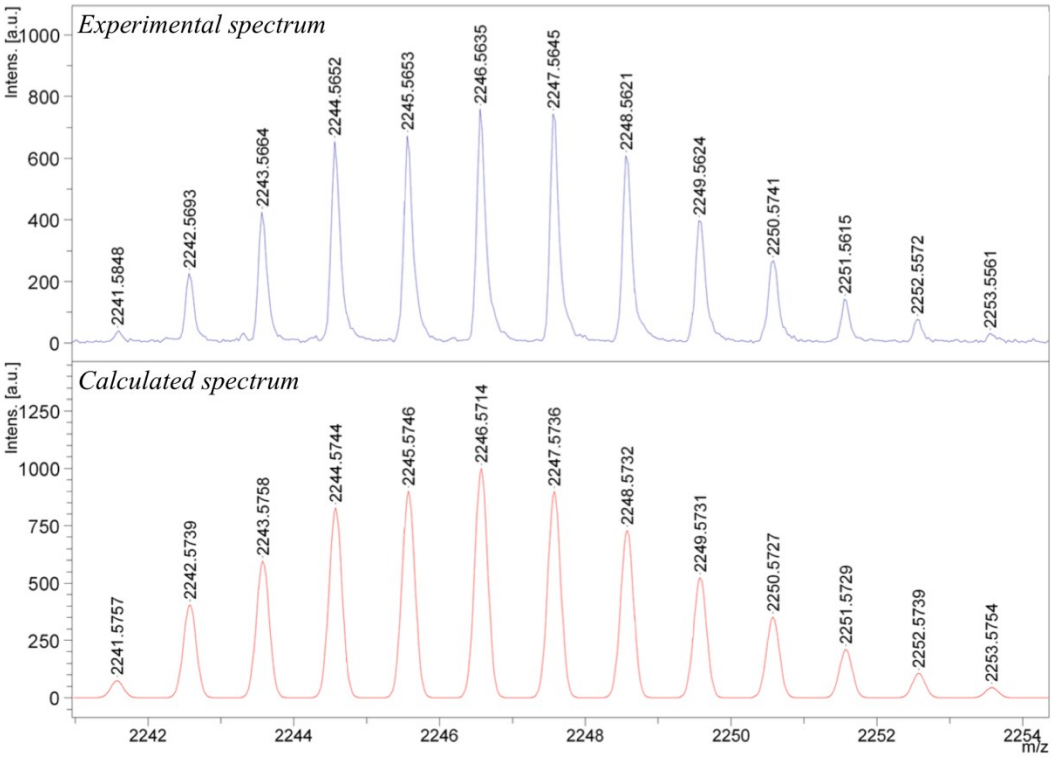

Fig. S13. HRMS MALDI/TOF spectrum of **4** (zoom)

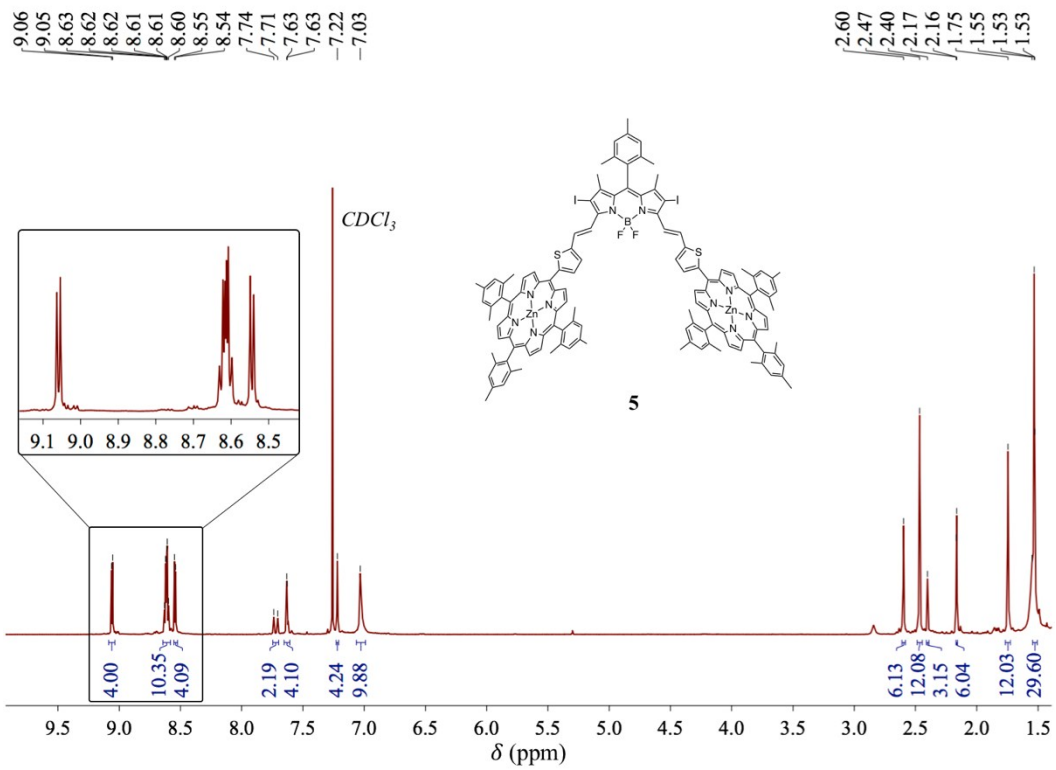

Fig. S14. ^{1}H NMR spectrum ($CDCl_3$, 500 MHz) of **5**

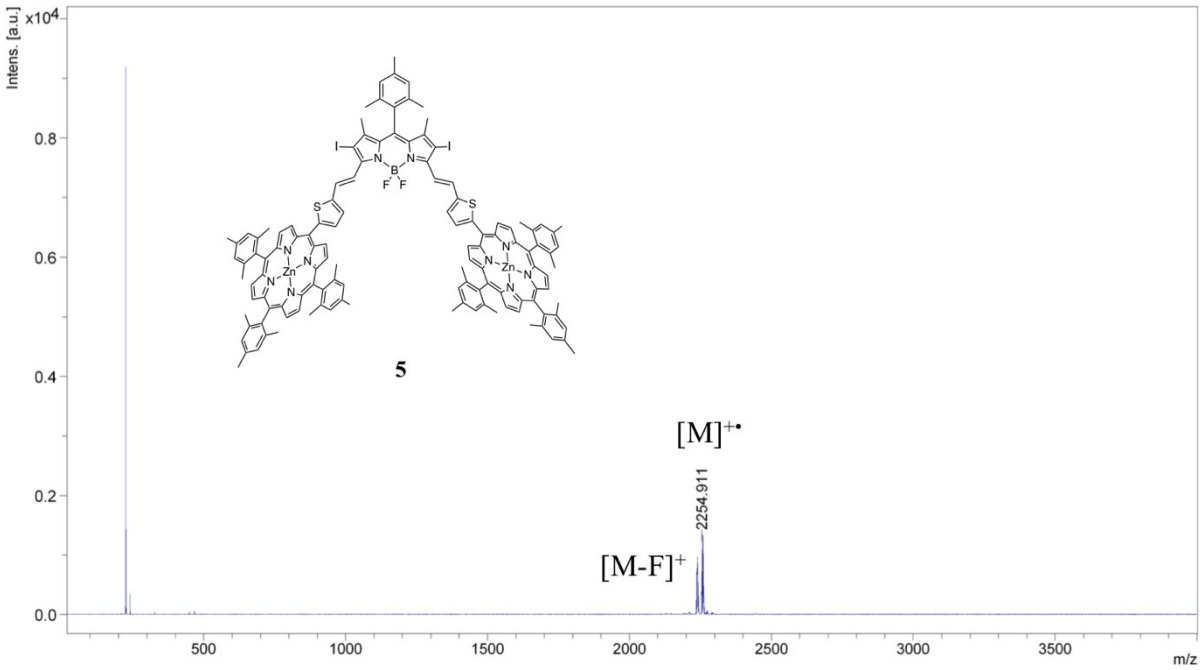

Fig. S15. LRMS MALDI/TOF spectrum of **5** (full)

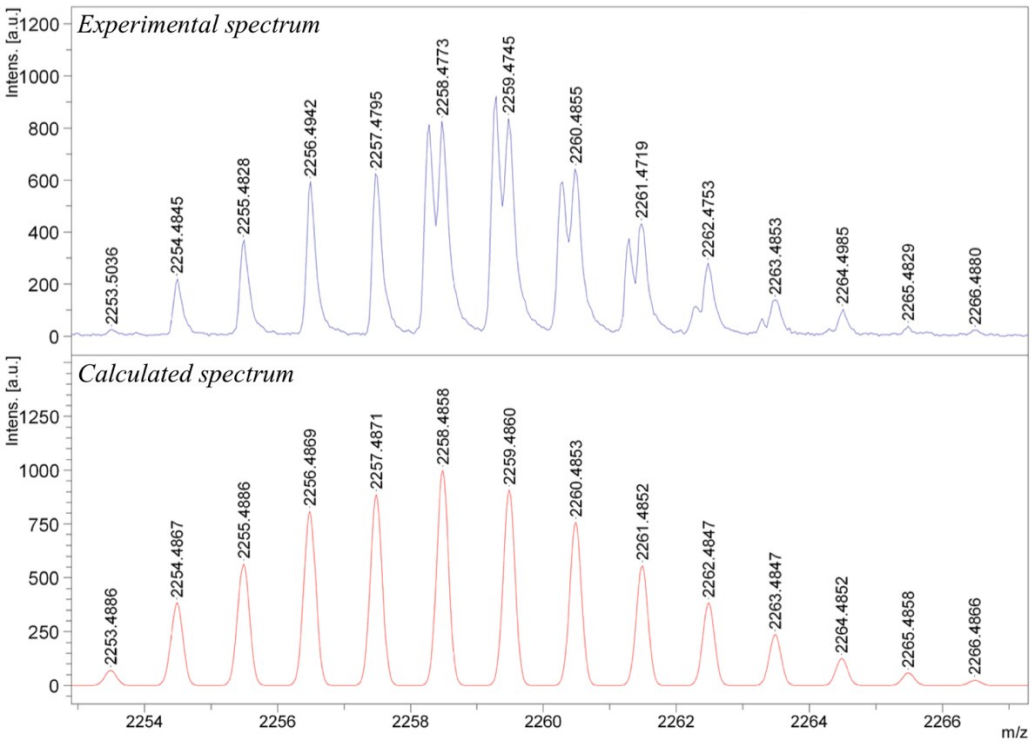

Fig. S16. HRMS MALDI/TOF spectrum of **5** (zoom)

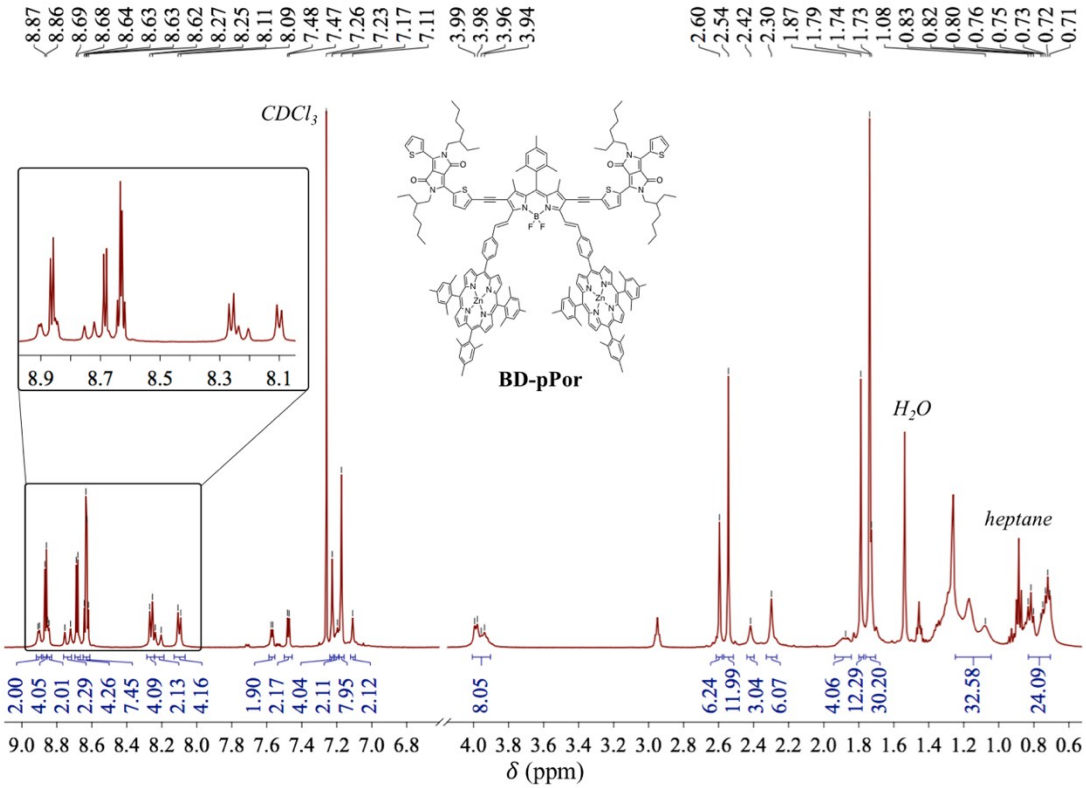

Fig. S17. ^{1}H NMR spectrum ($CDCl_3$, 500 MHz) of **BD-pPor**

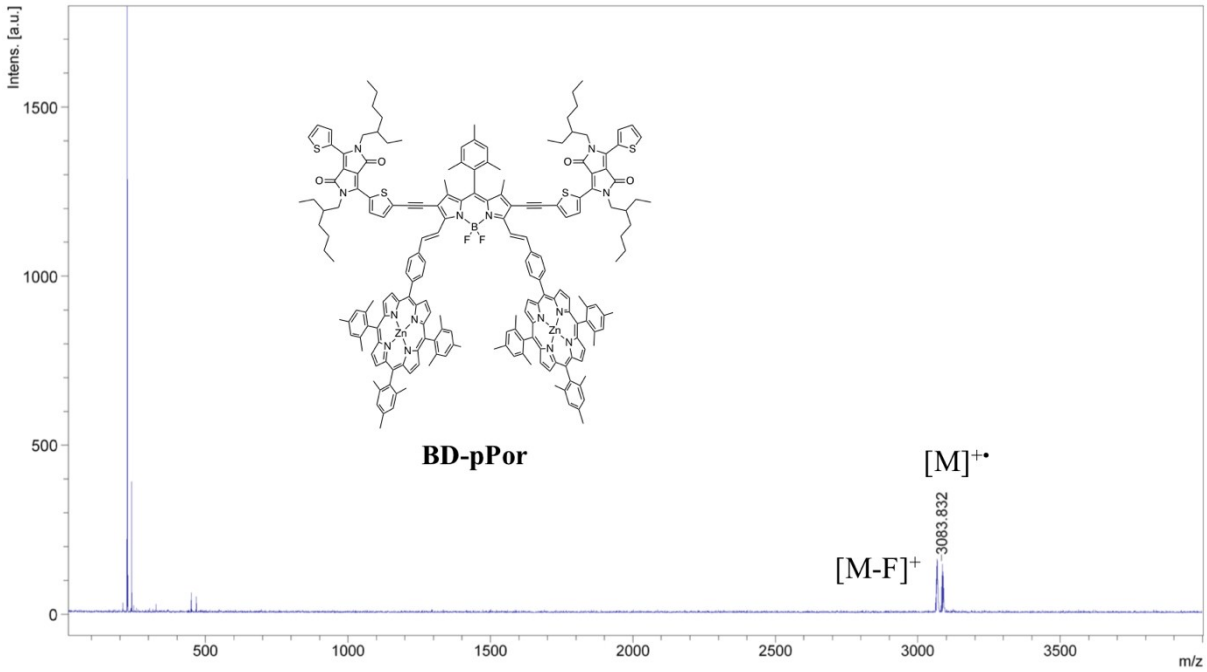

Fig. S18. LRMS MALDI/TOF spectrum of **BD-pPor** (full)

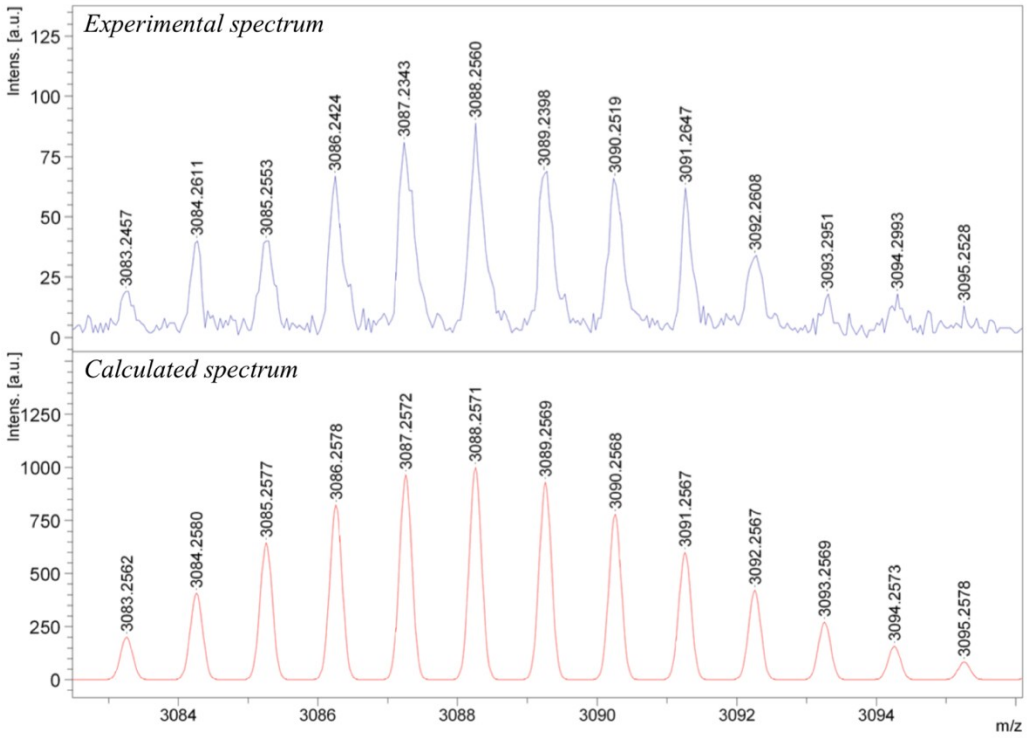

Fig. S19. HRMS MALDI/TOF spectrum of **BD-pPor** (zoom)

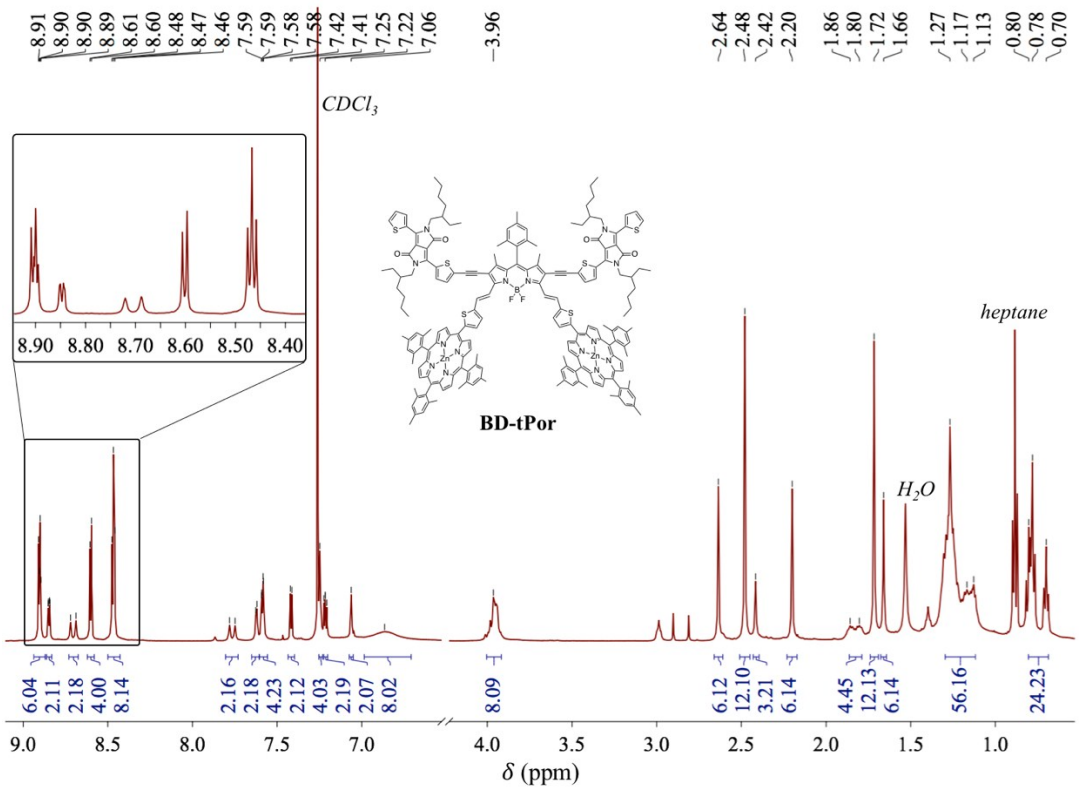

Fig. S20. ^{1}H NMR spectrum ($CDCl_3$, 500 MHz) of **BD-tPor**

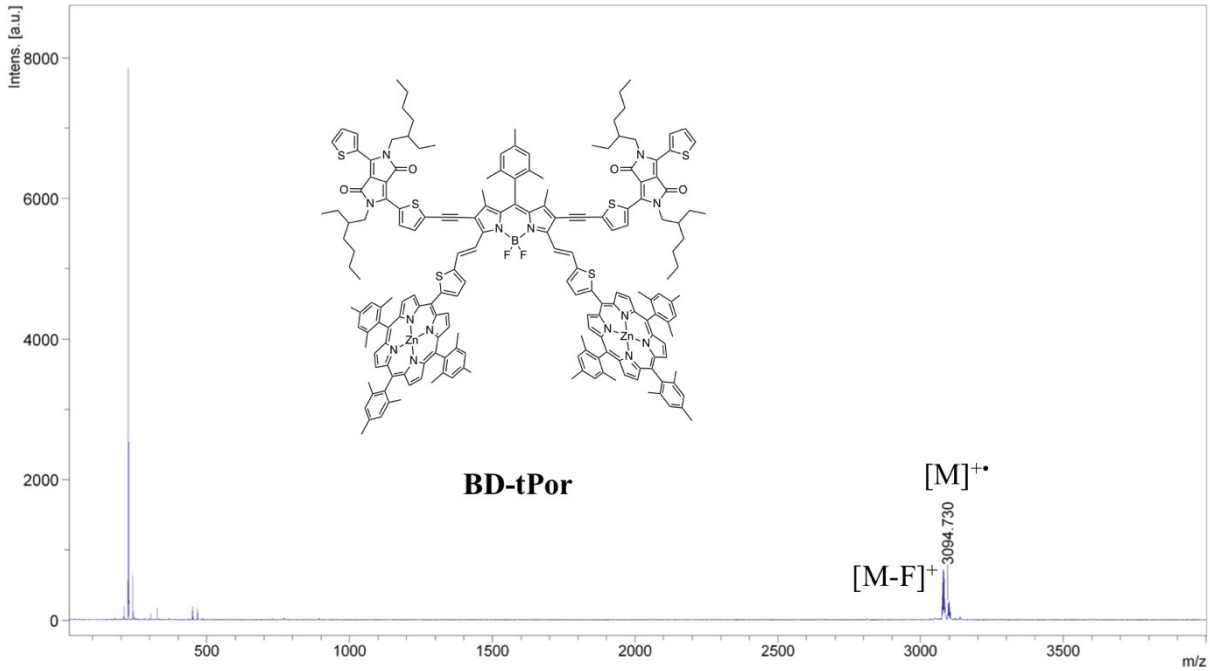

Fig. S21. LRMS MALDI/TOF spectrum of **BD-tPor** (full)

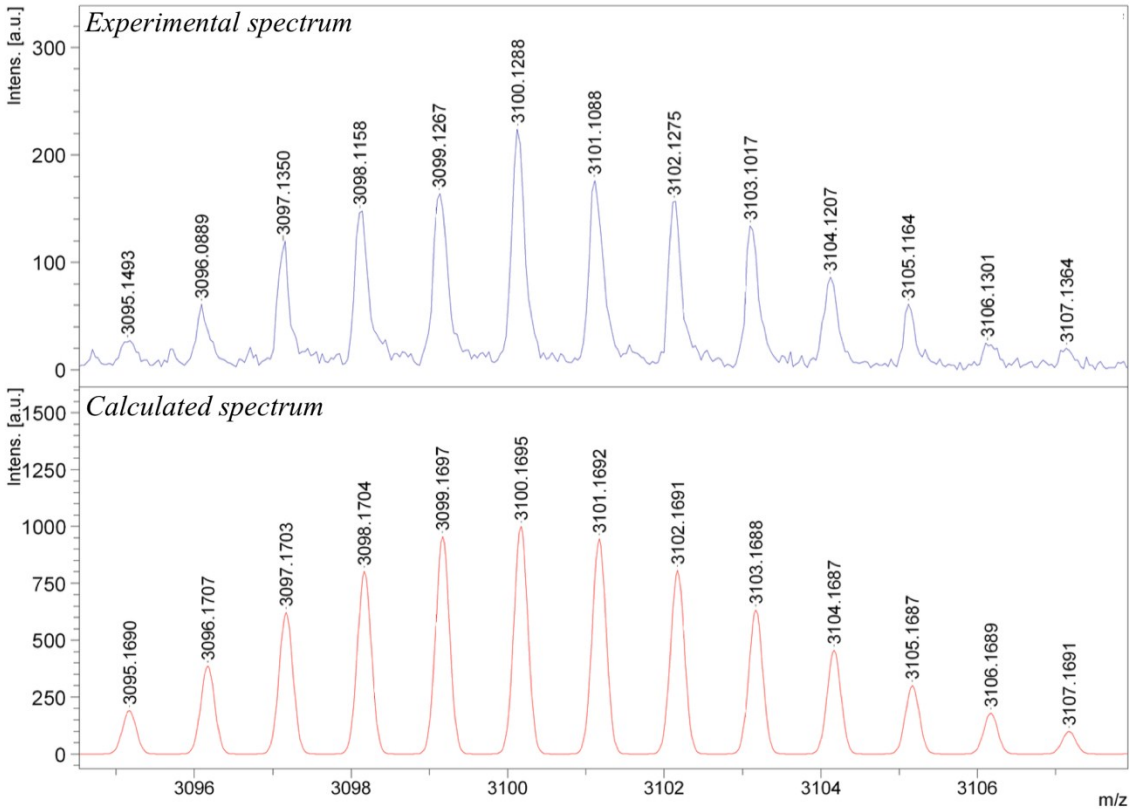

Fig. S22. HRMS MALDI/TOF spectrum of **BD-tPor** (zoom)

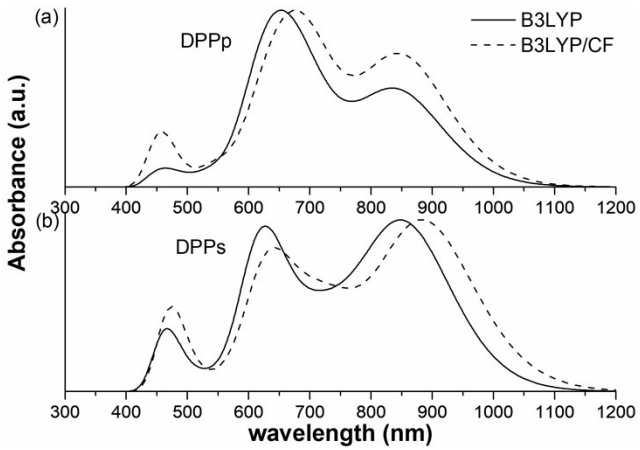

Fig. S23. Theoretical UV/Vis absorption spectrum of (a) **BD-pPor** and (b) **BD-tPor** (calculated using the B3LYP functional).

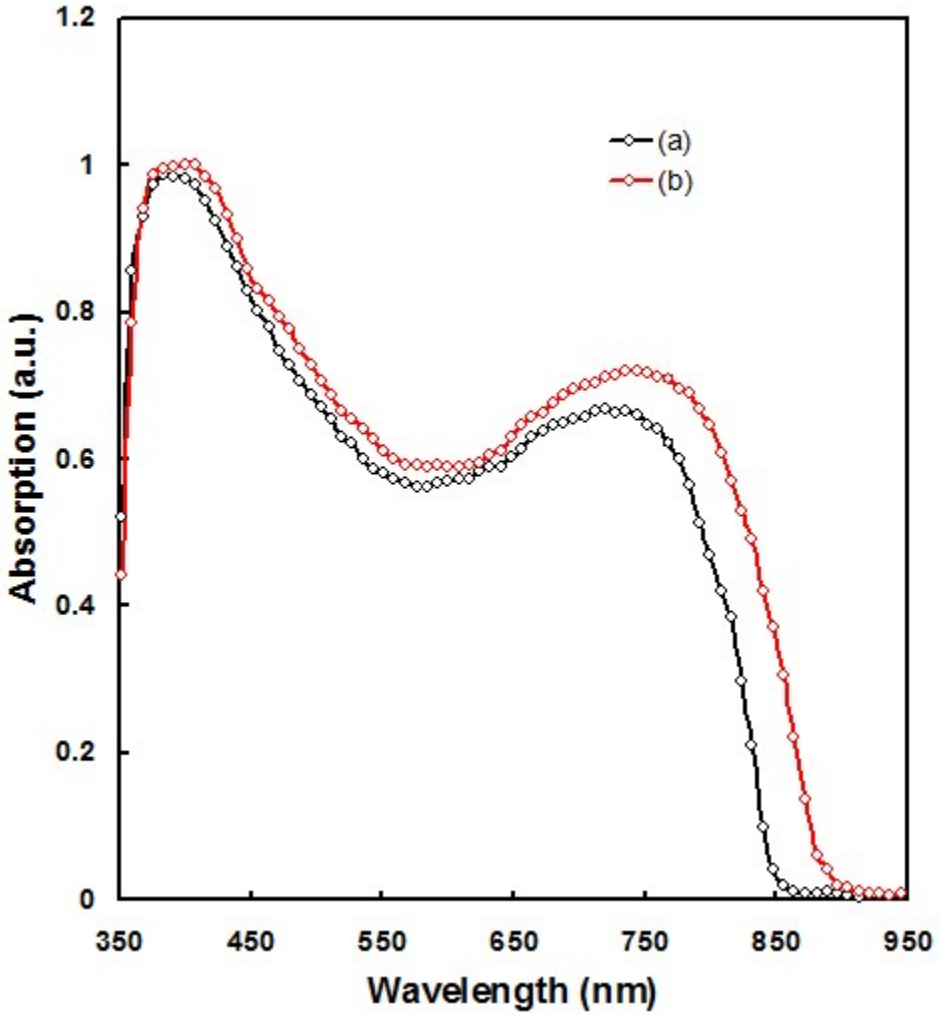

Fig. S24. Optical absorption spectra of (a) **BD-pPor**:$PC_{71}BM$ and (b) **BD-tPor**:$PC_{71}BM$ thin films

Table S1: Electronic excitations of **BD-pPor** (with non-negligible oscillator strengths, *f*), and the corresponding major contributions. Calculated using the M06 functional (and CF for solvent).

No.	Wavelength (nm)	*f*	Main Contributions
1	777.14	2.270	H→L (91%)
3	658.82	0.153	H–2→L (76%) H→L+1 (14%)
4	648.35	0.471	H–3→L (55%) H→L+2 (21%)
5	642.14	1.264	H→L+1 (57%) H–2→L (16%) H–1→L+2 (15%)
6	627.55	0.016	H→L+2 (48%) H–3→L (34%) H–1→L+1 (14%)
9	581.57	0.389	H–6→L (59%)
10	569.36	0.062	H–2→L+2 (19%) H–5→L+5 (13%) H–3→L+1 (14%) H–3→L+4 (11%)
11	565.39	0.010	H–2→L+3 (12%) H–6→L (20%) H–4→L+6 (16%) H–2→L+1 (14%) H–3→L+3 (12%)
13	556.78	0.019	H–4→L (26%) H–3→L+6 (23%) H–4→L+4 (17%) H–4→L+3 (11%)
14	556.08	0.068	H–2→L+6 (11%) H–1→L+2 (27%) H–2→L+1 (12%) H→L+1 (11%)
15	555.83	0.018	H–5→L (31%) H–2→L+5 (17%) H–5→L+3 (16%) H–3→L+5 (12%)
22	492.08	0.229	H→L+3 (72%)
23	490.73	0.014	H–6→L+1 (83%)
31	454.94	0.095	H–1→L+4 (53%) H–2→L+3 (31%)
34	449.32	0.019	H–10→L (48%) H–8→L (17%) H–3→L+3 (12%)
36	444.04	0.064	H–3→L+4 (21%) H–1→L+4 (21%) H–2→L+4 (19%) H–2→L+3 (15%)
37	443.10	0.636	H–7→L (78%)

Table S2: Electronic excitations of **BD-tPor** (with non-negligible oscillator strengths, *f*), and the corresponding major contributions. Calculated using the M06 functional (and CF for solvent).

No.	Wavelength (nm)	*f*	Main Contributions
1	826.12	2.568	H→L (93%)
2	682.66	0.580	H→L+1 (58%) H–2→L (25%)
3	674.27	0.548	H→L+2 (54%) H–3→L (23%)
4	665.15	0.157	H–1→L (92%)
5	657.11	0.381	H–2→L (68%) H→L+1 (22%)
6	639.49	0.053	H–3→L (71%) H→L+2 (23%)
8	589.89	0.657	H–2→L+1 (25%) H–4→L (14%) H–6→L (12%)
9	589.14	0.268	H–1→L+2 (12%) H–4→L (22%)
10	583.10	0.027	H–2→L+2 (28%) H–1→L+1 (21%) H–3→L+1 (12%)
11	576.24	0.041	H→L+3 (34%) H–1→L+1 (12%)
14	553.55	0.012	H–4→L (34%) H–5→L (19%)
15	552.14	0.029	H–5→L (36%) H–4→L (13%)
18	521.53	0.130	H→L+3 (36%) H–3→L+4 (13%) H–2→L+2 (12%) H–2→L+3 (12%)
20	517.46	0.011	H–2→L+2 (39%) H–3→L+1 (20%) H–3→L+2 (17%)
21	514.22	0.020	H→L+4 (45%) H–3→L+2 (14%) H–3→L+3 (14%)
22	505.07	0.021	H–5→L+1 (40%) H→L+5 (34%) H–4→L+2 (14%)
23	504.55	0.026	H→L+6 (35%) H–4→L+1 (22%) H–4→L+2 (17%)

			H–5→L+2 (14%)
			H–4→L+2 (29%)
24	499.07	0.015	H→L+5 (16%)
			H→L+6 (12%)
			H→L+6 (22%)
25	498.27	0.013	H→L+5 (16%)
			H–5→L+1 (14%)
27	487.63	0.041	H–6→L+2 (77%)
29	476.48	0.130	H–1→L+4 (56%)
			H–2→L+3 (26%)
32	463.42	0.408	H–7→L (77%)
			H→L+7 (10%)
			H–1→L+5 (51%)
33	462.54	0.025	H–1→L+6 (21%)
			H–2→L+6 (15%)
			H–1→L+6 (43%)
34	462.09	0.106	H–2→L+5 (21%)
			H–1→L+5 (17%)
			H–3→L+3 (25%)
35	454.40	0.034	H–2→L+4 (24%)
			H–8→L (20%)
			H–2→L+3 (30%)
36	452.83	0.110	H–1→L+4 (21%)
			H–3→L+4 (12%)
37	449.23	0.537	H→L+7 (51%)
			H–3→L+4 (21%)
38	448.49	0.016	H–8→L (61%)
			H–2→L+4 (19%)